

## Supplementary Information

### **High-sensitive CdTe Phototransistor with Response Spectrum Extended to 1.65 $\mu\text{m}$**

Jiyue Zhang,<sup>a,#</sup> Hechun Cao,<sup>a,#</sup> Wei Bai,<sup>a,\*</sup> Dongyang Zhao,<sup>a</sup> Yan Chen,<sup>a,c</sup> Xudong Wang,<sup>b,\*</sup> Jing Yang,<sup>a</sup> Yuanyuan Zhang,<sup>a</sup> Ruijuan Qi,<sup>a</sup> Rong Huang,<sup>a</sup> Xiaodong Tang,<sup>a,e,\*</sup> Jianlu Wang,<sup>b,c,d</sup> and Junhao Chu<sup>b,c</sup>

<sup>a</sup>*Key Laboratory of Polar Materials and Devices (MOE) and Department of Electronics, East China Normal University, Shanghai 200241, P.R. China*

<sup>b</sup>*National Lab for Infrared Physics, Shanghai Institute of Technical Physics, Chinese Academy of Sciences, Shanghai 200083, P.R. China*

<sup>c</sup>*Institute of Optoelectronics, Shanghai Frontier Base of Intelligent Optoelectronics and Perception, Fudan University, Shanghai 200433, China*

<sup>d</sup>*Hangzhou Institute for Advanced Study, University of Chinese Academy of Sciences, Chinese Academy of Sciences, Hangzhou 330106, China*

<sup>e</sup>*Collaborative Innovation Center of Extrem Optics, Shanxi University, Taiyuan, Shanxi 030006, P.R. China*

## Contents

**Fig. S1** Temperature dependence PL spectra of Cd-rich CdTe thin films.

**Fig. S2** PL spectra of CCT, TCT and NCT.

**Fig. S3** Diagram and optical microscope photographs of the transfer process.

**Fig. S4** TEM image of the transferred CdTe on SiO<sub>2</sub>/Si substrate.

**Fig. S5** Electrical properties of the T-CdTe thin film FETs.

**Fig. S6** Output characteristics under different light powers and at different gate voltages.

**Fig. S7** Output characteristics in darkness and illumination with various wavelengths.

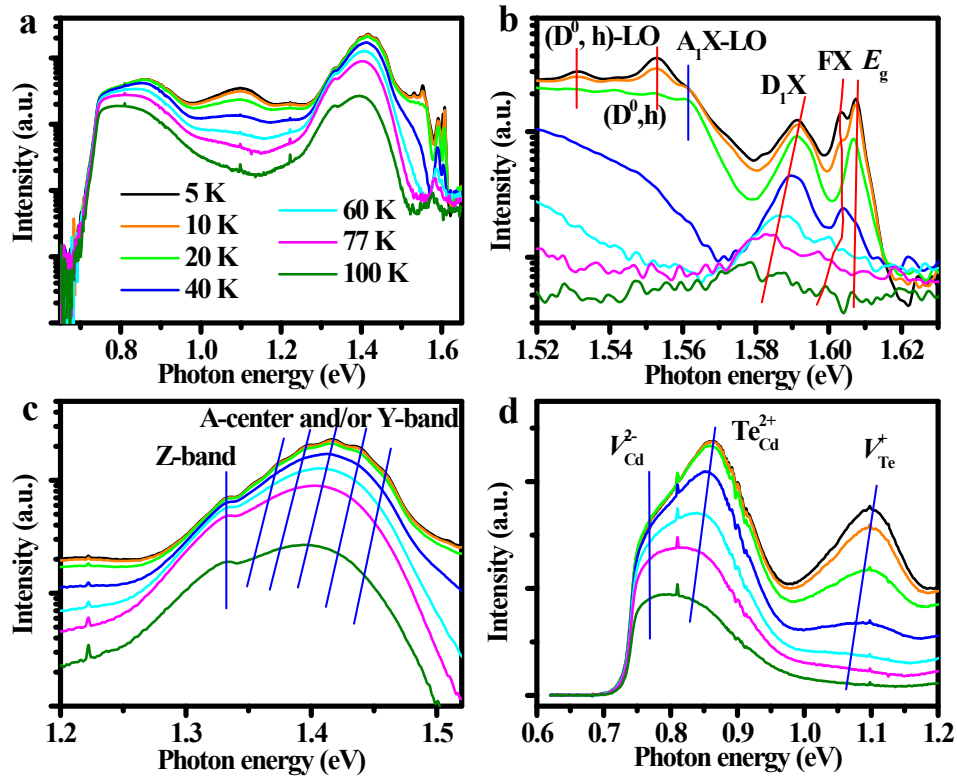
**Fig. S8** Output characteristics in darkness and light illumination with different incident light wavelengths.

**Fig. S9** Power dependency of  $D^*$  and  $EQE$  with wavelengths from 300 nm to 1.65  $\mu\text{m}$ .

**Fig. S10** Time-resolved photocurrent with selected wavelengths.

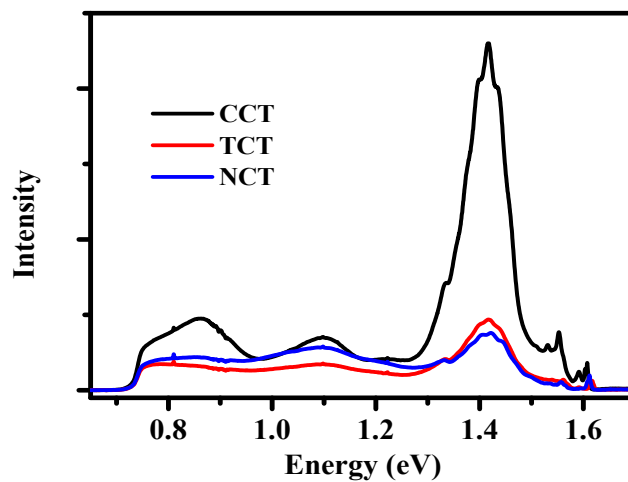
**Fig. S11** The rise and decay time of the photocurrent at selected wavelengths.

To clarify the possible origins of all PL peaks, the temperature dependence of PL spectra from 5 K to 100 K are studied and the data are plotted in Fig. S1a. Each transition at different energy regions can be assigned for similar transitions. As shown in Fig. S1b, the energy near 1.59 eV denoted as X-band is the free excitons (FX) and the excitons bound to neutral acceptors and donors ( $D_1X$  and  $A_1X$ -LO), in accordance with those of the polycrystalline and single crystalline CdTe samples.<sup>1-3</sup> The features around 1.55 eV are the donors to valence band ( $D^0, h$ ) and its phonon replicas denoted as ( $D^0, h$ )-LO, which were only reported in the Cd-rich CdTe materials.<sup>1-3</sup> As shown in Fig. S1c, a broad luminescence band around 1.45 eV is denoted as the Y-band, A-centre, and Z-band along with their LOs. The Y-band is attributed to the excitons bound to native structural defects, such as dislocations and stacking faults,<sup>1,2</sup> and the A-centre is a defect complex consisting of a  $V_{Cd}$  and a substitutional donor usually superposed with the Y-band correlated transition. The Z-band is related to the Z impurity rather than the dangling bonds on the core of dislocations.<sup>3</sup> The Z-band transition shows no noticeable shift with temperature range from 5 K to 100 K. However, an energy shift of 20 meV is obtained for the A-centre and/or Y-band, in complete agreement with those of the polycrystalline CdTe samples.<sup>3</sup> As shown in Fig. S1d, the 0.76 eV, 0.86 eV and 1.10 eV deep bands are attributed to  $V_{Cd}^{2-}$ ,  $Te_{Cd}^{2+}$  and  $V_{Te}^+$  defect, respectively.<sup>4,5</sup>



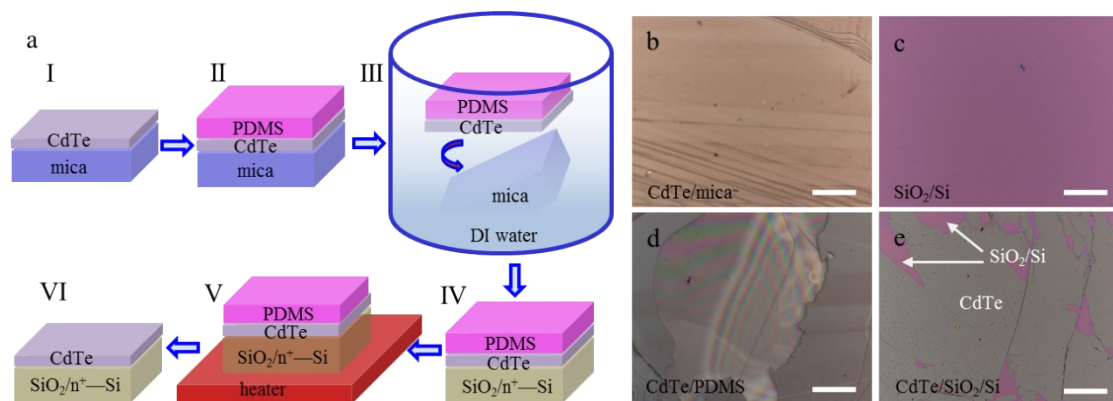
**Fig. S1** Temperature dependence PL spectra of Cd-rich CdTe thin films: (a) from 0.65 eV to 1.65 eV. (b) The DAP and exciton band. (c) The Z-band and A-center and/or Y-band. (d) The deep bands.

The PL spectra of the Cd-rich CdTe thin film (CCT), Te-rich CdTe thin film (TCT) and nominal CdTe thin film (NCT) are shown in Fig. S2. The emission lines of 0.76 eV, 0.8 eV and 1.1 eV are observed in CCT thin films.



**Fig. S2** PL spectra of CCT, TCT and NCT.

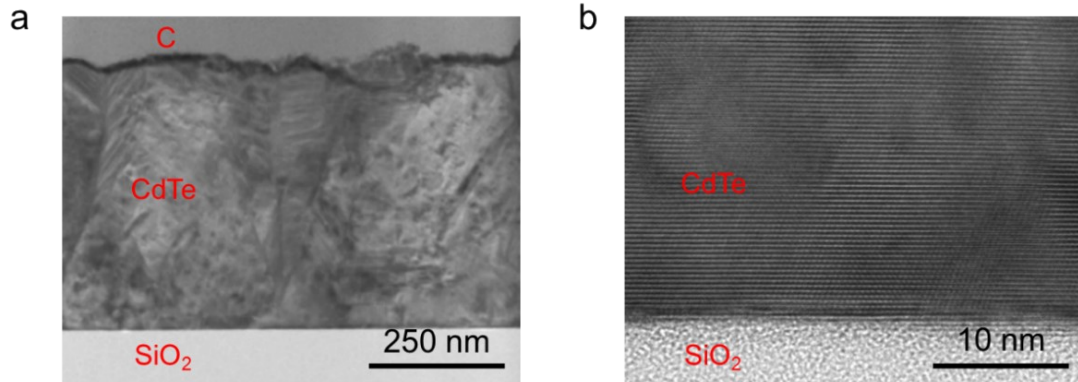
Fig. S3a shows a schematic diagram, where a water-assisted method is developed to peel off and transfer the vdWE CdTe thin film onto a heavy electron-doped silicon substrates covered with SiO<sub>2</sub>. Firstly, the film surface was cleaned with nitrogen gun to make it easier for PDMS stick on it. After the PDMS was covered on the surface of the film, the PDMS/CdTe/Mica was immersed in deionized water for 3 hours to break the van der Waals bonding between the Mica and CdTe. Subsequently, the PDMS/CdTe was separated from the Mica, taken out and transferred on Si/SiO<sub>2</sub> substrate. Finally, the PDMS/CdTe/SiO<sub>2</sub>/Si was placed on the heating plate for 10 minutes to remove the PDMS from the CdTe/SiO<sub>2</sub>/Si. Fig. S3b-e shows the optical images of the vdWE CdTe thin film on Mica, SiO<sub>2</sub>/Si substrate, CdTe thin film attached to PDMS after separated from Mica substrate, and CdTe thin film transferred to SiO<sub>2</sub>/Si substrate, respectively. The optical images implied that the large-area transferable films (denoted as T-CdTe) with hundred microns scale were realized. The largest scale of the CdTe thin films by exfoliation and transfer can be achieved to be 0.4 mm × 0.4 mm.



**Fig. S3** The scheme illustration (a) and optical microscope photographs for the transfer process (b)-(e) (Scale bar: 50 $\mu$ m).

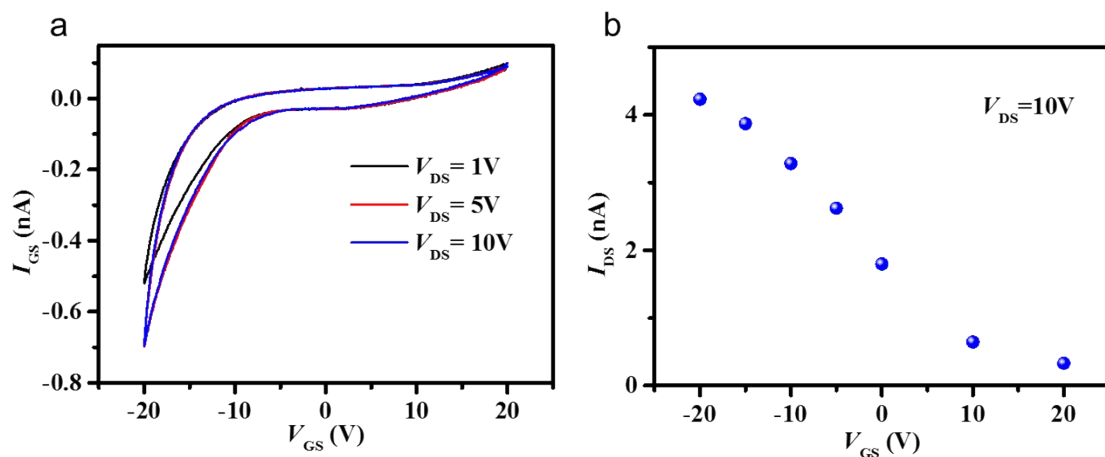
Fig. S4a shows that the interface between T-CdTe and SiO<sub>2</sub> is clear, flat and free of

impurities. Fig. S4b shows the perfect lattice fringe. The HRTEM images demonstrate the high-quality crystallinity is maintained for the vdWE CdTe after transfer.



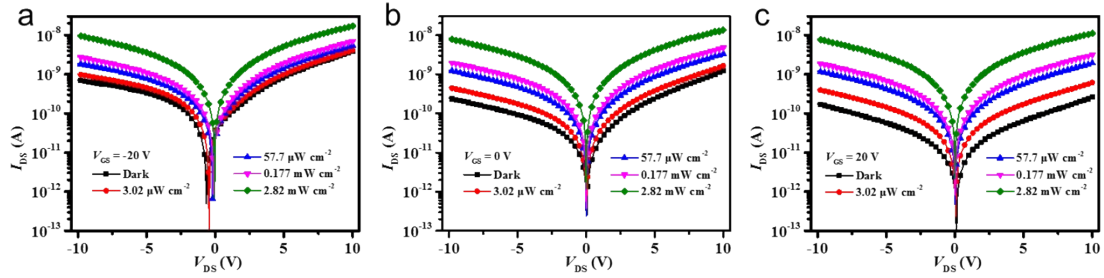
**Fig. S4** TEM image of the transferred CdTe on SiO<sub>2</sub> substrate. (a) Low-magnification TEM image. (b) HRTEM image.

The weak leakage current of  $I_{GS}$  shown in Fig. S5a guarantees the carrier control by a gate voltage, and also rules out the contribution of  $I_{GS}$  on the  $I_{DS}$  and photogenerated currents. Fig. S5b shows the plot of the  $I_{DS}$  with  $V_{GS}$  extracted from Fig. 2b at  $V_{DS} = 10$  V, similar to those of the transfer characteristic curves, which also confirms the p-type behavior of the vdWE CdTe thin film.



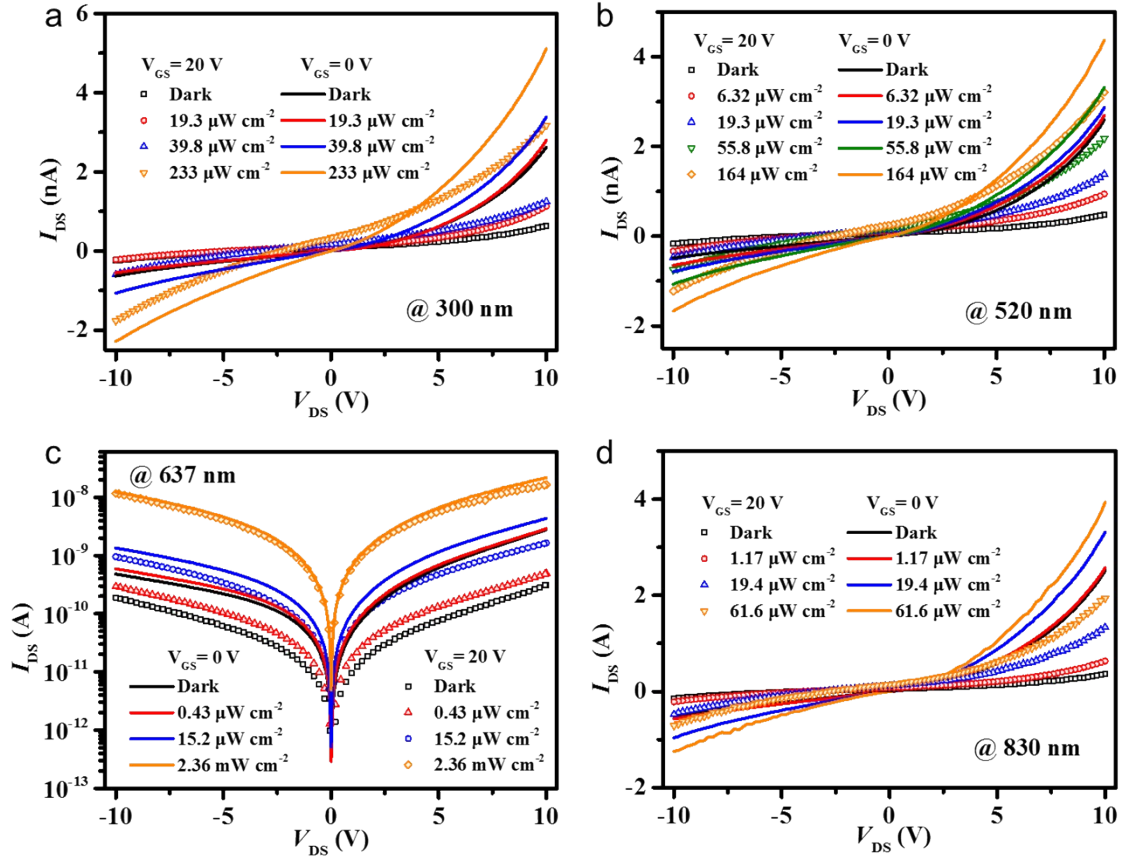
**Fig. S5** Electrical properties of the T-CdTe thin film FETs. (a) The transfer curve extracted from Fig. 2b. (b) The  $I_{GS}$  as a function of  $V_{GS}$ .

Fig. S6a-c show the output characteristic traces under different light powers at  $V_{GS} = -20$  V,  $V_{GS} = 0$  V and  $V_{GS} = 20$  V, respectively. It is clear that the dark current is suppressed by applying a positive gate, which leads to a larger photoswitching on/off ratio and a improved photo detection sensitivity.



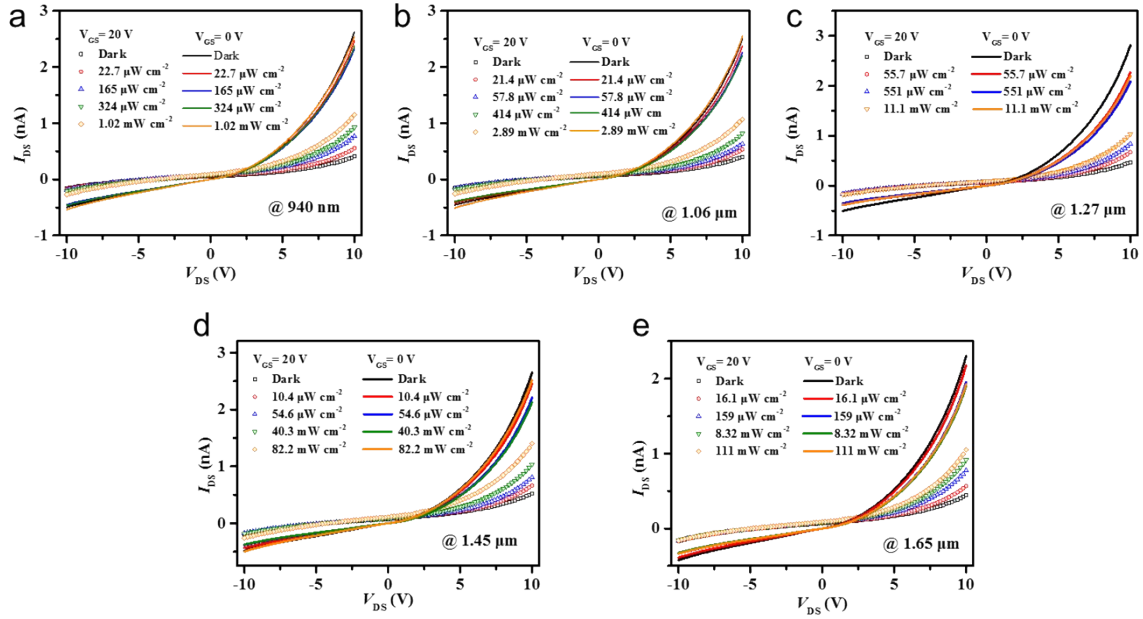
**Fig. S6** Output characteristics under different light powers at (a)  $V_{GS} = -20$  V, (b)  $V_{GS} = 0$  V and (c)  $V_{GS} = 20$  V.

Fig. S7a-d show show the output characteristic curves in darkness and different light illumination at  $V_{GS} = 0$  V and  $V_{GS} = 20$  V with incident light wavelengths of 300 nm, 520 nm, 637 nm and 830 nm, respectively. Clearly, the hole concentrations are effectively suppressed by applying a positive gate, which can bring out the improvement of the  $D^*$ .



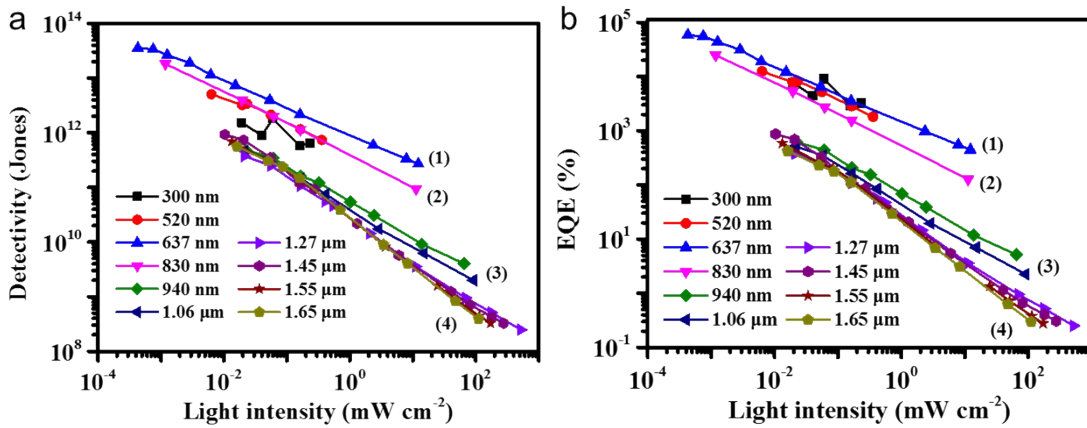
**Fig. S7** Output characteristics in darkness and light illumination at  $V_{GS} = 0$  V and  $V_{GS} = 20$  V with incident light wavelengths of (a) 300 nm, (b) 520 nm, (c) 637 nm and (d) 830 nm.

Fig. S8a-e show the output characteristic curves in darkness and different light illumination at  $V_{GS} = 0$  V and  $V_{GS} = 20$  V with incident light wavelengths of 940 nm, 1.06  $\mu\text{m}$ , 1.27  $\mu\text{m}$ , 1.45  $\mu\text{m}$  and 1.65  $\mu\text{m}$ , respectively. Note that the  $I_{DS}$  is independent on the illumination intensity when the  $V_{GS}$  is set to be 0 V, implying that negligible and even no photoresponse is present without a gate at the extended wavelength region.



**Fig. S8** Output characteristics in darkness and light illumination at  $V_{GS} = 0 V$  and  $V_{GS} = 20 V$  with incident light wavelengths of (a) 940 nm, (b) 1.06  $\mu m$ , (c) 1.27  $\mu m$ , (d) 1.45  $\mu m$  and (e) 1.65  $\mu m$ .

The power dependency of  $D^*$  and  $EQE$  with incident light wavelengths from 300 nm to 1.65  $\mu m$  are summarized in Fig. S9. Clearly, both the power dependency of  $D^*$  (Fig. S9a) and  $EQE$  (Fig. S9b) can be divided into four categories according to photon energy similar to those plotted in Fig. 5a and b, namely (1)  $E_{\text{photon}} > E_g$ , (2)  $E_{\text{photon}} \sim E_g$ , (3)  $1.1 \text{ eV} < E_{\text{light}} < E_g$ , and (4)  $0.8 \text{ eV} < E_{\text{light}} < 1.1 \text{ eV}$ , in good agreement with the PL emission positions as displayed in Fig. 1a.



**Fig. S9** The power dependency of  $D^*$  (Fig. S9a) and EQE (Fig. S9b) with incident light wavelengths from 300 nm to 1.65  $\mu\text{m}$ .

The time-resolved photocurrents at the selected representative wavelengths are given in Fig. S10a-e. Clearly, highly stable and reliable photoswitching between the low and the high conductivity are found all in these regions, confirming the good mechanical behaviors of the T-CdTe photodetectors under a gate voltage of 20 V in the extended spectrum.

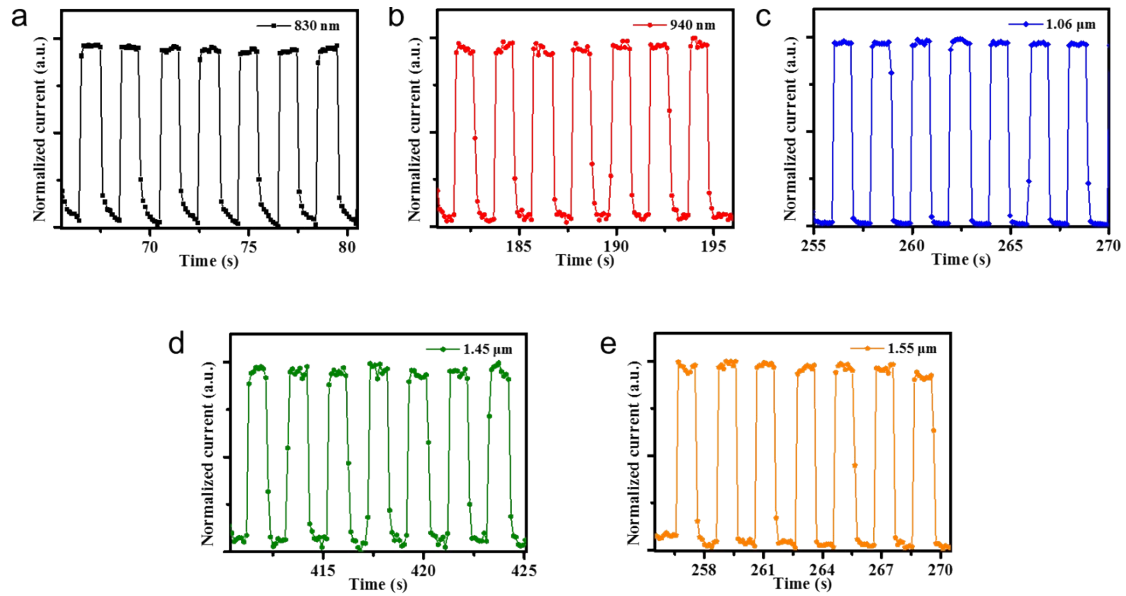


**Fig. S10** Time-resolved photocurrent with incident light wavelengths of (a) 830 nm, (b) 940 nm, (c) 1.06  $\mu\text{m}$ , (d) 1.45  $\mu\text{m}$  and (e) 1.55  $\mu\text{m}$ .

The response time for the representative wavelengths is measured to evaluate the lifetime of the photogenerated carrier  $\tau_{\text{ph}}$ . Fig. S11 show the rising and fall of the photocurrent and the fitted data using exponential functions with incident light wavelengths of (a) 830 nm, (b) 940 nm, (c) 1.06  $\mu\text{m}$  and (d) 1.55  $\mu\text{m}$ , respectively. It is clear that the response time for the 830 nm is the shortest and reaches around 200  $\mu\text{s}$ , which is in good agreement with the transition mechanisms as displayed in the inset of

Fig. 5d. In addition, the response rising times for the other wavelengths are around 3.4 ms, 3.17 ms and 3.82 ms, respectively. These results reflect a fast response behavior in the extended wavelength region. The fast photoswitching feature are much superior to those of the CdTe nanorods phototransistors ( $\tau_{\text{rising}}/\tau_{\text{decay}} = 1.1 \text{ s}/(3.3 + 17.1) \text{ s}$ )<sup>6</sup> and of the CdTe nanosheets photodetectors ( $\tau_{\text{rising}}/\tau_{\text{decay}} = 18.4 \text{ ms}/14.7 \text{ ms}$ ).<sup>7</sup>

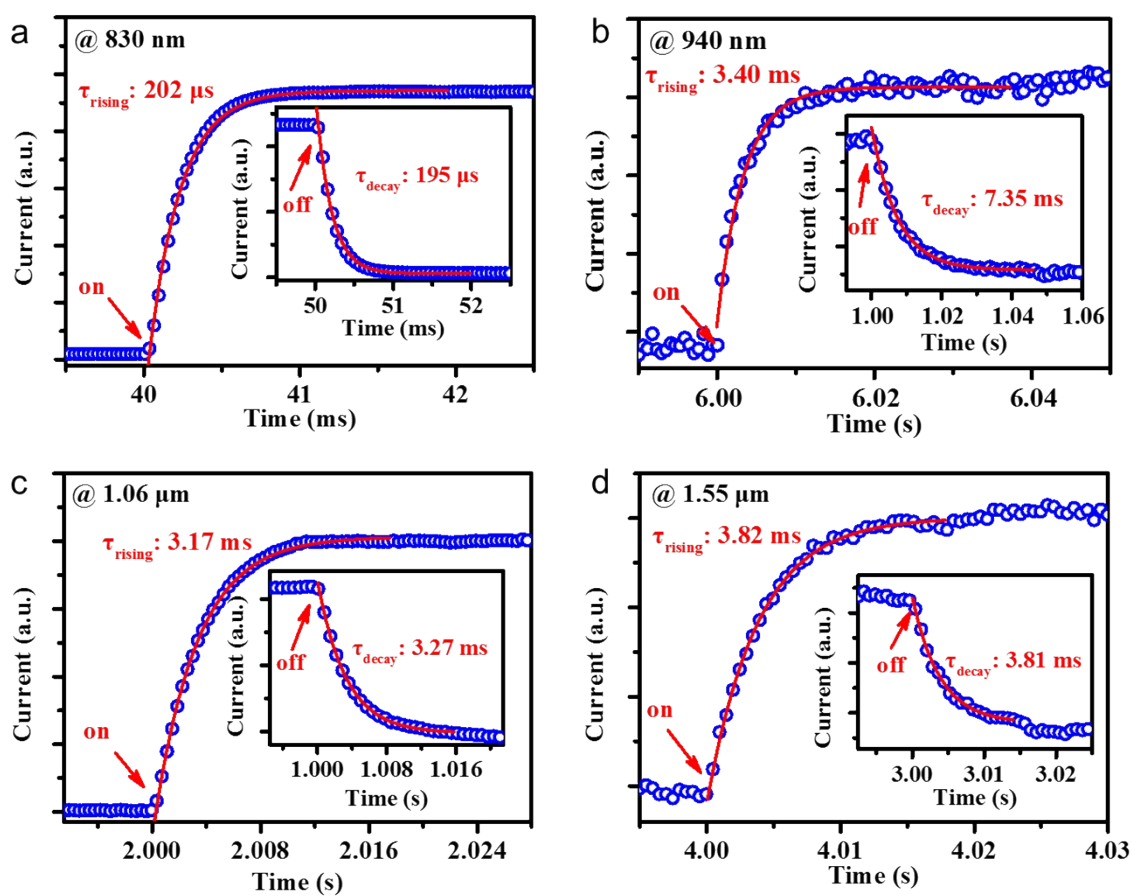


**Fig. S11** The rise and fall of the photocurrent and the fitted data using exponential functions with incident light wavelengths of (a) 830 nm, (b) 940 nm, (c) 1.06  $\mu\text{m}$  and (d) 1.55  $\mu\text{m}$ .

## References

1. D. S. Albin, D. Kuciauskas, J. Ma, W. K. Metzger, J. M. Burst, H. R. Moutinho and P. C. Dippo, *Appl. Phys. Lett.*, 2014, **104**, 092109.
2. D. P. Halliday, M. D. G. Potter, J. T. Mullins and A. W. Brinkman, *JJ. Cryst. Growth*, 2000, **220**, 30-38.
3. C. Kraft, H. Metzner, M. Hädrich, U. Reislöhner, P. Schley, G. Gobsch and R. Goldhahn, *J. Appl. Phys.*, 2010, **108**, 124503.
4. A. Castaldini, A. Cavallini, B. Fraboni, P. Fernandez and J. Piqueras, *J. Appl. Phys.*, 1998, **83**, 2121-2126.
5. A. Wardak, M. Szot, G. Janusz, D. Kochanowska, M. Witkowska-Baran and A. Mycielski, *J. Lumin.*, 2021, **231**, 117833.
6. X. Xie, S. Y. Kwok, Z. Lu, Y. Liu, Y. Cao, L. Luo, J. A. Zapien, I. Bello, C. S. Lee, S. T. Lee and W. Zhang, *Nanoscale*, 2012, **4**, 2914-2919.
7. R. Cheng, Y. Wen, L. Yin, F. Wang, F. Wang, K. Liu, T. A. Shifa, J. Li, C. Jiang, Z. Wang and J. He, *Adv. Mater.*, 2017, **29**, 1703122.